Journal Pre-proof

Biodegradable SPI-based hydrogel for controlled release of nanomedicines: a potential approach against brain tumors recurrence

Francesca Viale, Matilde Ciprandi, Luca Leoni, Giulia Sierri, Antonio Renda, Federica Barbugian, Marcus Koch, Silvia Sesana, Lucia Salvioni, Miriam Colombo, Francesco Mantegazza, Laura Russo, Francesca Re
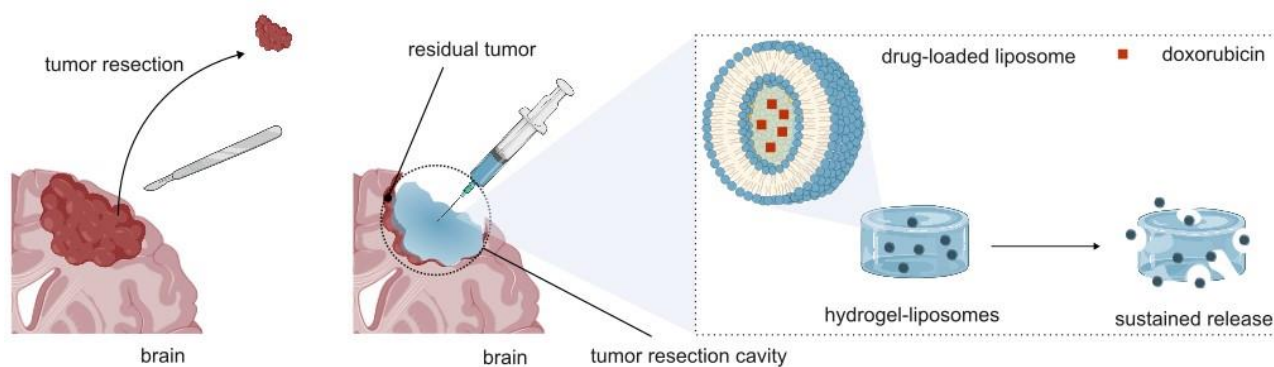
Please cite this article as: F. Viale, M. Ciprandi, L. Leoni, G. Sierri, A. Renda, F. Barbugian, M. Koch, S. Sesana, L. Salvioni, M. Colombo, F. Mantegazza, L. Russo, F. Re, Biodegradable SPI-based hydrogel for controlled release of nanomedicines: a potential approach against brain tumors recurrence, *Journal of Drug Delivery Science and Technology*, https://doi.org/10.1016/j.jddst.2024.105672.

Scheme 1-Graphical Abstract. Illustration of the proposed strategy to counteract GB recurrence. After surgical resection of the newly diagnosed GB, SPI hydrogel embedding drug-loaded liposomes will be implanted for the controlled release of nanomedicines.

Biodegradable SPI-based hydrogel for controlled release of nanomedicines: a potential approach against brain tumors recurrence

Francesca Viale [a†], Matilde Ciprandi [a†], Luca Leoni [a], Giulia Sierri [a], Antonio Renda [a], Federica Barbugian [b], Marcus Koch [c], Silvia Sesana [a], Lucia Salvioni [b], Miriam Colombo [b], Francesco Mantegazza [a], Laura Russo [a,d], Francesca Re [a] *

[a] School of Medicine and Surgery, University of Milano-Bicocca, 20854 Monza, Italy

[b] Department of Biotechnology and Biosciences, University of Milano-Bicocca, 20126 Milano, Italy

[c] INM-Leibniz Institute for New Materials, Campus D2 2, 66123 Saarbrücken, Germany

[d] CÚRAM, SFI Research Centre for Medical Devices, National University of Galway, H91 W2TY Galway, Ireland

† Equally contribution

* Correspondence to: francesca.re1@unimib.it

Email addresses: f.viale1@campus.unimib.it; m.ciprandi2@campus.unimib.it; l.leoni6@campus.unimib.it; g.sierri@campus.unimib.it; a.renda3@campus.unimib.it; f.barbugian@campus.unimib.it; Marcus.Koch@leibniz-inm.de; mariasilvia.sesana@unimib.it; lucia.salvioni@unimib.it; miriam.colombo@unimib.it; francesco.mantegazza@unimib.it; laura.russo@unimib.it; francesca.re1@unimib.it

Abstract

Glioblastoma (GB) is the most common and aggressive brain tumor. The treatment for newly diagnosed glioblastoma is surgical resection of the primary tumor mass, followed by radiotherapy and chemotherapy. However, recurrences frequently occur in proximity to the surgical resection area. In these cases, none of the current therapies is effective. Recently, implantable biomaterials seem to be a promising strategy against GB recurrence. Here, for the first time we combined the tailorable properties of soy-protein hydrogels with the versatility of drug-loaded liposomes to realize a hybrid biomaterial for controlled and sustained nanoparticles release. Hydrogel consisting of 18-20% w/v soy-protein isolated were fabricated in absence of chemical cross-linkers. They were biodegradable (-10% and -30% of weight by hydrolytic and enzymatic degradation, respectively in 3 days), biocompatible (>95% of cell viability after treatment), and capable of sustained release of intact doxorubicin-loaded liposomes (diffusion coefficient between 10^{-18} and 10^{-19} m^2 s^{-1}). A proof-of-concept in a "donut-like" 3D-bioprinted model shows that liposomes released by hydrogels were able to diffuse in a model with a complex extracellular matrix-like network and a 3D structural organization, targeting glioblastoma cells.

The combination of nanoparticles' encapsulation capabilities with the hydrogels' structural support and controlled release properties will provide a powerful tool with high clinical relevance that could be applicable for the treatment of other cancers, realizing patient-specific interventions.

KEYWORDS

Hydrogel, nanoparticles, glioblastoma, brain, liposomes, biomaterial.

1. Introduction

Glioblastoma (GB) is a devastating malignant neoplasm characterized by a poor prognosis, with a median overall survival lower than two years and a five-year survival rate below 10% [1]. Currently, the standard of care for the treatment of GB involves maximal surgical resection followed by concurrent radiation therapy (RT) and temozolomide (TMZ) for 6 weeks, then adjuvant TMZ for 6 months, accordingly to Stupp's protocol [2]. Nevertheless, GB remains one of the most treatment-resistant brain malignancies, with a 90% of recurrence rate by six months after resection [3]. Currently, there are four FDA-approved treatments mainly used against recurrent GB: lomustine, intravenous carmustine, bevacizumab, and tumor treatment fields (TTFields) [4]. However, it remains chemotherapy-resistant, with higher invasiveness and aggressiveness compared with the original tumor [1], partially due to tumor heterogeneity and limited drug access to the brain for the presence of the blood–brain barrier (BBB) [5,6]. Indeed, the achievement of a sufficient conveyance across the BBB is a key challenge for biopharmaceutical molecules that are excluded from the brain [7]. In this context, nanoparticles can be used as permeation enhancers to boost drugs into the brain. Nanoparticles are investigated as drug delivery platforms from several decades, and the first nanoformulation for cancer therapy, based on liposomes, was approved more than 20 years ago [8]. Liposomes have excellent biocompatibility and effective drug delivery of lipophilic, hydrophilic and amphiphilic drugs [9]. However, there are not yet nanoscale medicines approved for brain indications, but some of them are currently under study for the treatment of brain tumors [10]. Much more extensive research is needed in order to have nanoparticles capable of delivering drugs to the brain in quantities that are pharmacologically effective, before to reach human application.

Considering that malignant gliomas rarely metastasize outside the brain, one alternative approach to the systemic administration that allows BBB dodging is the direct administration of drugs in the tumor resection area [11]. In this context, implantable biomaterials for controlled drug release are an emerging field in medical research and healthcare. These biomaterials offer several advantages over traditional drug delivery methods, including localized and controlled release, reduced systemic side effects, improved patient compliance, and enhanced therapeutic efficacy [12]. There are various types of biomaterials that include implantable colloidal carriers, polymeric-based delivery system (e.g. films or wafers), and hydrogels that can be implanted or injected in the brain along the walls and floor of the resection cavity [13–15]. Currently, there is only one FDA-approved device for the treatment of newly-diagnosed and recurrent GB, known commercially as Gliadel® wafer. This is a biodegradable co-polymer in which the anticancer agent carmustine is incorporated into a matrix made of 1,3-bis(p-carboxyphenoxy)propane and sebacic acid [16]. However, Gliadel® wafers showed several disadvantages such as poor drug diffusion, fast drug release and several post-surgical adverse events in treated patients [17].

Recently, the combination of nanoparticles' encapsulation capabilities with the hydrogels' structural support and controlled release properties provides a powerful tool with high clinical relevance [18]. Different implants are developing for the local treatment of GB [19,20], including μMESH loaded with docetaxel-nanoparticles and diclofenac [13], and hydrogels loaded with nanoparticles carrying anti-cancer drugs. These approaches showed promising results in preclinical GB models, increasing significantly the median survival time of the animals and delaying the tumor [21–24].

However, limitations concerning the risk benefit ratio, the scale up of implants and the limited drug penetration and distribution in the diseased area still exist.

Among the different types of nanoparticles that can be loaded in implantable biomaterials, liposomes are compatible with hydrogels composed by chitosan [25], cross-linked poly(acrylic acid) (PAA) such as Carbopol [26], agar/gelatin [27] and poly lactic-co-glycolic acid [28], hyaluronic acid [29]. However, at the best of our knowledge, there are no data on the liposomes loading in soy protein-based hydrogels for biomedical purposes, in particular against GB relapse. In the last years, the utilization of soy protein-based hydrogels in drug delivery practices is growing because they hold the advantages of both natural and synthetic polymers [30]. The soy protein is abundant in nature, easy to isolate, biocompatible and biodegradable [31,32]. These hydrogels can be fabricated without the use of chemical modifiers or crosslinkers, and the jellification can occur at physiological temperature (i.e. 37°C) [32].

In this study, we combined for the first time fully-based soy protein isolate (SPI) hydrogels with doxorubicin-loaded liposomes, as a nanomedicine model, for the potential treatment of recurrent GB. The idea underneath this study is to generate an implantable *in situ*-gelling gel, easy to be produced on large scale and in the absence of cross-linkers, that fits the post-surgical cavity properly, capable to release in a sustained manner the embedded nanomedicines and biodegradable to avoid intracranial hypertension or other adverse reactions (Scheme 1-Graphical Abstract).

2. Materials and Methods

2.1 Preparation of hydrogels

Soy protein isolate (SPI) (MP Biomedicals, LLC, Solon, OH, USA) was solubilized in Dulbecco's

Phosphate Buffer Saline (D-PBS: 133 mg/L calcium chloride, 100 mg/L magnesium chloride, 200

mg/L potassium chloride, 200 mg/L potassium phosphate, 8000 mg/L sodium chloride, 1143. 56

mg/L sodium phosphate - Merck KGaA, Darmstadt, Germany) or artificial CSF (aCSF) at a

concentration of 10, 15, 18, and 20% w/v [32]. aCSF was prepared according to the recipe available

from Cold Spring Harbor without the addition of gaseous CO_2 and O_2 [33,34].

The resulting suspensions were homogenized at 12000 rpm, RT (Ultra-Turrax T25, IKA) and

dispensed into 24-well plates, 0.5 g of suspension per well, using a 5-mL syringe without a needle.

Plates were incubated for 30 min at 37°C in 5% CO_2 humidity to promote gelation and then the

formation of hydrogels (Supplementary Fig. 1). The hydrogels produced were of two types: those

used for biomaterial characterization, containing only SPI and those used for hydrogel validation,

loaded with liposomes. Liposomes ([total lipids] ranging from 100 to 200 μM, see 2.8) were added

to D-PBS buffer used to solubilize SPI. A minimum of 10 batches were prepared for each type of

hydrogels.

2.2 Water absorption capacity and swelling of hydrogels

To assess the SPI's ability to absorb aqueous solutions, the hydrogels were weighed after gelation

(Wi). Samples were lyophilized to obtain the final dry weight (Wd). The percentage of D-PBS or

aCSF absorbed by SPI was calculated by the following equation:

$$\% D - PBS \ = \ \frac{Wi - Wd}{Wi} x \ 100$$

Next, the swelling capacity of the gelled sample was measured. The hydrogels were submerged in 2 mL of buffer solutions and then maintained at 37°C under humid conditions. In this case, each hydrogel was weighed prior to the addition of buffer solutions (Wi) and at the end of different time points (Wf). The following equation was used to calculate the % swelling:

$$\% \; swelling \; = \frac{Wf - Wi}{Wi} \; x \; 100$$

2.3 Cryo-EM imaging of SPI solution

For cryogenic transmission electron microscopy (cryo-EM) 3 µl of SPI solution (18% or 20% w/v in D-PBS) were placed on a holey carbon supported copper grid (Plano, Wetzlar, Germany, type S147-4), blotted for 2 s and vitrified using a Gatan (Pleasanton, CA, United States) CP3 cryo-plunge freezing instrument operating at -165 °C. The sample was transferred to a Gatan model 914 cryo-EM sample holder and analyzed with a JEOL (Tokyo, Japan) JEM-2100 LaB$_6$ TEM at 200 kV accelerating voltage. TEM bright field micrographs were acquired using a Gatan Orius SC1000 CCD camera working under low-dose conditions.

2.4 Rheological tests

SPI hydrogels were prepared as described above. Immediately after the gelation (30 min at 37°C), hydrogels were analysed at 25 °C using a rotational rheometer (Modular Compact Rheometer MCR 72, Anton Paar, Graz, Austria). Steady-state shear flow from 0.1 to 1000 s^{-1} of shear rate was performed. The results are expressed as viscosity depending on the applied shear rate for hydrogels at 25 °C [35]. The dependence of the stress on the shear rate was also determined and the yield point was calculated according to Bingham's law [36]

7

2.5 Hydrolytic degradation of hydrogels

The degradation of hydrogels in D-PBS (or aCSF) was determined.

Hydrogels were prepared as described above and incubated with 2 mL of buffer solutions at 37°C

for different time points up to 72 h. At the end of each time point, every sample was taken and

lyophilized to obtain the dry weight of gel (Wd). The amount of SPI released from hydrogels into

buffer solution is expressed as a % of weight loss using the following equation:

$$\% \ weight \ loss \ = \frac{Wi - Wd}{Wi} x100$$

where Wi is the amount of initial SPI used for the production of individual samples. As

corroboration, the amount of SPI present in D-PBS (or aCSF) after hydrolytic degradation of the

hydrogels was quantified by the bicinchoninic acid (BCA) colorimetric assay (Pierce BCA Protein

Assay kit, Thermo Fisher Scientific, Waltham, Massachusetts, USA).

2.6 Enzymatic degradation of hydrogels

The enzymatic degradation of hydrogels was monitored following the same protocol above

described, but in this case, hydrogels were maintained in a buffer solution added with 1600 µg/mL

of activated Kallikrein-related peptidase 6 (KLK6, Recombinant Human Kallikrein 6,

rhKLK6/Neurosin, R&D system Bio-Techne, 614 McKinley Place NE Minneapolis, MN,USA).

KLK6 was activated by lysyl-endopeptidase (Merck KGaA, Darmstadt, Germany) in 50 mM Tris,

0.05% w/v Brij-35, pH 8.0 buffer at room temperature for 30 minutes, following manufacturer's

instruction. KLK6 was used because it is abundantly expressed in the central nervous system and

it has also been detected at high levels in human cerebrospinal fluid [37–40]

2.7 Preparation and characterization of liposomes

Conventional liposomes were prepared by extrusion through 50, 100, 150 and 400-nm polycarbonate membrane filters [41]. Briefly, 5 mM of sphingomyelin and cholesterol (Sigma-Aldrich, St. Louis, Missouri, USA) in a molar ratio of 1:1 (M:M), added or not with 0.5 mol% of fluorescent Bodipy®-sphingomyelin or 1 mol% of fluorescent Rhodamine-phosphatidylethanolamine (Invitrogen, Waltham, Massachusetts, USA) were dissolved in chloroform in a round-bottom flask and mixed for 5 min. Then a phospholipid film was obtained through evaporation with a rotary evaporator. The resulting dried lipid film was hydrated for about 2 h by addition of D-PBS above the lipid phase transition temperature (55 °C). After hydration, unilamellar liposomes were obtained by extrusion.

Doxorubicin-loaded liposomes (LIPO-DOX) were prepared as described [42]. Briefly, sphingomyelin-cholesterol liposomes were prepared by extrusion through 100 nm-pore size filters in ammonium sulfate (500 mM, pH 5.5) and then dialyzed against 10 mM Hepes, 150 mM NaCl pH 7.4 overnight. Doxorubicin (DOX) was added to liposomes (2.7 μmol DOX/10 μmol total lipids) and its incorporation in the liposomes core was allowed by heating at 65 °C and ultrasounds. Unloaded DOX was removed by ultrafiltration, drug loading was quantified spectrofluorimetrically after vesicle disruption with HEPES 0.1% Triton X-100 and lipid recovery was measured by Stewart's assay [42].

Size, polydispersity index (PDI) and ζ-Potential were analyzed by dynamic light scattering (DLS) equipped with a ZetaPALS device (Brookhaven Instruments Corporation, Holtsville, NY, USA) as previously described [43]. Liposomes morphology was assessed by cryo-EM [43].

2.8 Characterization of hydrogel embedding liposomes

To characterize hydrogels embedding liposomes, SPI was dissolved in D-PBS added with 0.1 mM Rhodamine B and with Bodipy-loaded liposomes (100 nmol/ml total lipids). Images were acquired using the Operetta CLS High Content Analysis System (Perkin Elmer, Waltham, MA, USA) equipped with 20x water objective and standard instrument filters as per the manufacturer's protocol using the live imaging tool.

In order to evaluate the effective liposomes release from the hydrogel, liposomes (100 µM) were added to the D-PBS used for the preparation of hydrogels (see 2.1 section). After gelation, hydrogels were submerged in 2 mL of D-PBS and incubated at 37°C. At different time points (up to 72 h), the D-PBS was collected and the amount of released liposomes was measured by Nanoparticle Tracking Analysis (NTA, NanoSight NS300, Malvern Panalytical, Salisbury, UK) [42]. In this case, the D-PBS solution in which the hydrogels were immersed was taken at the selected time points, centrifuged at 15,000 RPM for 30 min at 4° C to minimize the presence of SPI particulate matter that might have interfered with the quantification of the liposomes by NTA. To obtain the kinetic profile of release from hydrogels for up to 6 days, the number of released liposomes was measured as a function of time. The resulting data were fitted with a sigmoidal function f(t):

$$f(t) = A - A/(1 + Exp[(t - t_1)/S_0])$$

where t is the time measured after the beginning of the release and A, t_1, and S_0 free fitting parameters. Namely A represents the normalization asymptotic value, t_1 is the time corresponding at half of the total release, and S_0 corresponds to the steepness of the sigmoidal function.

10

The mesh size determines the diffusion through the hydrogel. If the size of the mesh is larger than the size of the drug ($r_{mesh}/r_{drug} > 1$), the drug is released by diffusion and the time of diffusion is higher when the mesh size approaches the drug size ($r_{mesh}/r_{drug} \sim 1$). On the contrary, if the drug size is larger than the mesh size ($r_{mesh}/r_{drug} < 1$), the release of the drug depends on the degradation of the hydrogel [15]. Therefore, we estimate the diffusion coefficient D by using this equation:

$$D = \frac{k_B T}{6\pi\eta r_{drug}}$$

where k_B is Boltzmann constant, η is the medium viscosity, and T is the absolute temperature. These data allowed us to corroborate the type of release and to assess liposomes' movement rate.

2.9 Cell culture

The U87-MG cell line was used as an *in vitro* model of GB. Cells were maintained in culture in in Dulbecco's Modified Eagle Medium (DMEM) High Glucose w/o sodium pyruvate (ECM0101L, Euroclone, Milan, Italy) supplemented with 10% fetal bovine serum (FBS, ECS0180L, Euroclone, Milan, Italy), 4 mM L-glutamine (ECB3000D, Euroclone, Milan, Italy), and 100 U/mL penicillin/streptomycin (P/S) (ECB3001B, Euroclone, Milan, Italy). Cultured cells were maintained at 37°C in a humidified environment and 5% CO_2. The NHA (Normal Human Astrocytes, Lonza) were cultured in complete Astrocytes' Basal Medium as described [44].

2.9 Cell viability assay and astrogliosis evaluation

To evaluate the biocompatibility of SPI, U87-MG cells were plated in a 96-well multiwell (18˙000 cells/well) and treated with D-PBS conditioned from 24 h hydrolytic degradation of hydrogels, for 72 h, at 37°C. To evaluate the biocompatibility of SPI on NHA cells, as model of healthy brain, cells were plated in a 96-well multiwell (15˙000 cells/well) and treated with different doses of SPI

dissolved in culture medium for 24 h, at 37°C. Moreover, the potential SPI-induced astrogliosis was verified by measuring the GFAP levels of NHA cells as described [PMID: 35008528], after treatment with 2 mg/ml of SPI. Briefly, after incubation cells were lysed in RIPA buffer. Then, 10 μg of total proteins was loaded into gel pre-cast 4-12% Bis-Tris followed by immunoblotting analysis using anti-GFAP antibody (1:1500, Dako, Milano, Italy). GFAP bands were visualized by an enhanced chemiluminescence system using Amersham Imager 600 (GE Healthcare Srl, Milano, Italy). All the data were normalized to α-vinculin (anti- α -vinculin 1:1000, Cell Signalling, Milano, Italy).

U87-MG cells were treated with LIPO-DOX, both from the original preparation or released from the hydrogel after 24 h, to evaluate their anti-tumor capacity. Cells were treated with liposomes containing 5 µg/mL, 10 µg/mL or 25 µg/mL of DOX for 72 h at 37°C, 5% CO_2. At the end of incubation, cell viability was assessed by MTT assay as described [41]. Cell viability was calculated compared with untreated cells used as control (100% viability).

Results are presented as the mean of three independent standard deviation experiments.

2.10 Preparation of "donut-like" 3D-bioprinted model

The 3D-bioprinted GB model was generated as already reported [45]. Briefly, a hybrid ink based on gelatin (GE-MF, gelatin functionalized with methyl-furan), chitosan (CH-MF, chitosan functionalized with methyl-furan) and maleimide-star-PEG (PEG-Star-MA) was generated by Diels-Alder reaction. GE-MF (66 mg) and CH-MF (34 mg) were dissolved in 1.5 mL of PBS at 37 °C and vortexed until complete dissolution. PEG-Star-MA (5 mg) was dissolved in 0.5 mL of PBS at RT, added to the GE-CH hybrid solution, and mixed. The GE-CH solution was left for 30 min under UV light for further sterilization and 2 h at 37 °C to obtain partial network formation of

the hydrogel solution. U87-MG cells (4×10^6/mL) in complete medium were added to the GE-CH solution (3 mL) to formulate the final bioink and transferred into a 5 mL bioprinter syringe. Each construct was bioprinted as an empty cylinder (donut) on 24 multiwell plate using a 22 G nozzle with a 0.41 mm diameter at 50 kPa. After printing, cells were maintained at 37 °C with 5% CO_2. The culture media were refreshed every day for 5 days.

2.12. Proof-of-concept *in vitro* using 3D-bioprinted models

SPI-hydrogels loaded with fluorescent Rhodamine-LIPO were injected in the cavity of 3D-bioprinted models. After different time of incubation, the cell viability in the 3D-bioprinted constructs was evaluated using a calcein/Hoechst ^{TM} viability kit (Invitrogen), following the manufacturer's instructions. Briefly, 1 mL of calcein/Hoechst solution was added to each bioprinted construct (3 µL calcein and 4 µL Hoechst in 12 mL of PBS). After 40 min of incubation at 37 °C, the stained bioprinted models were washed three times with PBS before image acquisition. Imaging analysis was performed with a confocal microscopy 10× Ph objective, with a Z-stack of 6.6 µm each slice.

Cell viability (V) % was calculated as reported in Eq. 1:

$$V\ (\%) = n/N*100 \qquad\qquad\qquad (Eq.\ 1)$$

Where n = number of living cells and N = number of total cells.

2.11 Statistical analysis

Each experiment was conducted at least in triplicate, and data were expressed as mean ± standard deviation (SD). Statistical analyses were performed with GraphPad Prism 8, using one-way and two-way ANOVA by Tukey's test. Statistical significance was considered at $p < 0.05$.

3. Results and Discussion

The current standard treatment of GB still results in a poor prognosis for recurrent patients. Therefore, other therapeutic strategies and novel interventions should be developed. Local delivery of chemotherapeutics and/or adjuvant agents poses an interesting route to potentially improve the GB outcomes. Among them, biomaterials for controlled release of therapeutics are well suited to applications against GB recurrence.

In this scenario, our proposal is to generate a natural, biocompatible and biodegradable hydrogel that can be introduced directly inside the post-surgical cavity for controlled release of nanomedicines with the final aim to reduce the possibility of GB recurrence (Scheme 1-Graphical Abstract).

Pure SPI-based hydrogels were physically fabricated by a heating gelation process. Five SPI densities (10, 15, 18 and 20 % w/v) were utilized to prepare hydrogels. In order to obtain an SPI solution suitable for injection (i.e. not too thick and not too liquid), 18 and 20% w/v of SPI were selected.

Cylindrical hydrogels of 1.5±2 cm diameter, 1±0.5 cm high and 0.5±0.02 g weight were obtained. Hydrogels showed light brown color with an overall homogenous appearance (Supplementary Fig. 1). The hydrogels formation is based on electrostatic interactions, disulfide bonding and hydrogen bonding between SPI subunits, as described [32]. Hydrogels were characterized by determining water absorption and swelling capability. Results showed that the water content of 18 and 20%

14

w/v SPI hydrogels significantly decreased, 81.67±% and 78.15± % respectively (Figure 1A), as the protein content increased accordingly to the literature [32]. The high water content of hydrogels contributes to their softness and flexible consistency, which are key parameters to avoid a mechanical mismatch between the biomaterial and the soft brain tissue [46].

Using Cryo-EM microscopy, an image of the morphology and internal structure of hydrogels was obtained (Figure 1B). Hydrogels exhibit protein networks and pores that can allow the passage of fluids allowing the absorption and subsequent swelling of the hydrogels, as well as allowing the release of nanoparticles to the external environment. Pores of approximately 25-100 nm were visible, likely due to air bubbles introduced during the SPI homogenization, as suggested by Chien et al [32]. No significant differences were observed between 18% w/v and 20% w/v hydrogels.

Considering that the brain consists of roughly 80% water [47], it is important to determine the swelling behavior of hydrogels because it represents a critical parameter that can affect the intracranial hypertension following the implant. The swelling % of hydrogels was determined by soaking them in D-PBS and measuring the weight increase over time. 18 and 20% w/v hydrogels were subjected to swelling, actually hydrogels' weight increased by about 20% in 1 h. After that time, hydrogels' weight remains constant over time. At longer times the swelling tended to decrease (i.e. ~11% at 72 h), probably due to hydrolytic degradation of the hydrogels (Figure 1C). This result suggests that hydrogels retain a significant aqueous fraction within their structure without dissolving in water. After swelling, no appreciable changes in size of hydrogels were observed. Almost the same results were obtained substituting D-PBS with aCSF, a buffer solution with a composition representative of cerebrospinal fluid [33,34].

To investigate the mechanical properties of hydrogels, a rotational rheometer was used. In the steady-state flow test, it was observed that the viscosity of hydrogels decreased very markedly

with the increasing shear rate, indicating a pronounced shear-thinning behavior (Figure 1D), as reported for other type of hydrogels [48]. The viscosity of SPI hydrogels decreases of about five orders of magnitude as the shear rate increases from 0.1 to 1000 s^{-1}. Such strong shear thinning is a highly desirable feature to make materials injectable through syringes, while the rapid recovery to high viscosity leads to high shape fidelity [48,49].

A better picture of the hydrogel's flow behavior can be gained from the stress–shear rate portion (Figure 1E), from which it is possible to determine the yield point, i.e. the critical shear rate value required for the destruction of the spatial network, after which the hydrogel is able to exhibit fluidity [50]. The results showed that the yield point increases with an increase in the concentration of the SPI, from 602 Pa for the 18% to 860 Pa for the 20% w/v hydrogels. These values are in the range of stiffness of normal brain tissue that is 0.1 to 1 kPa [51,52].
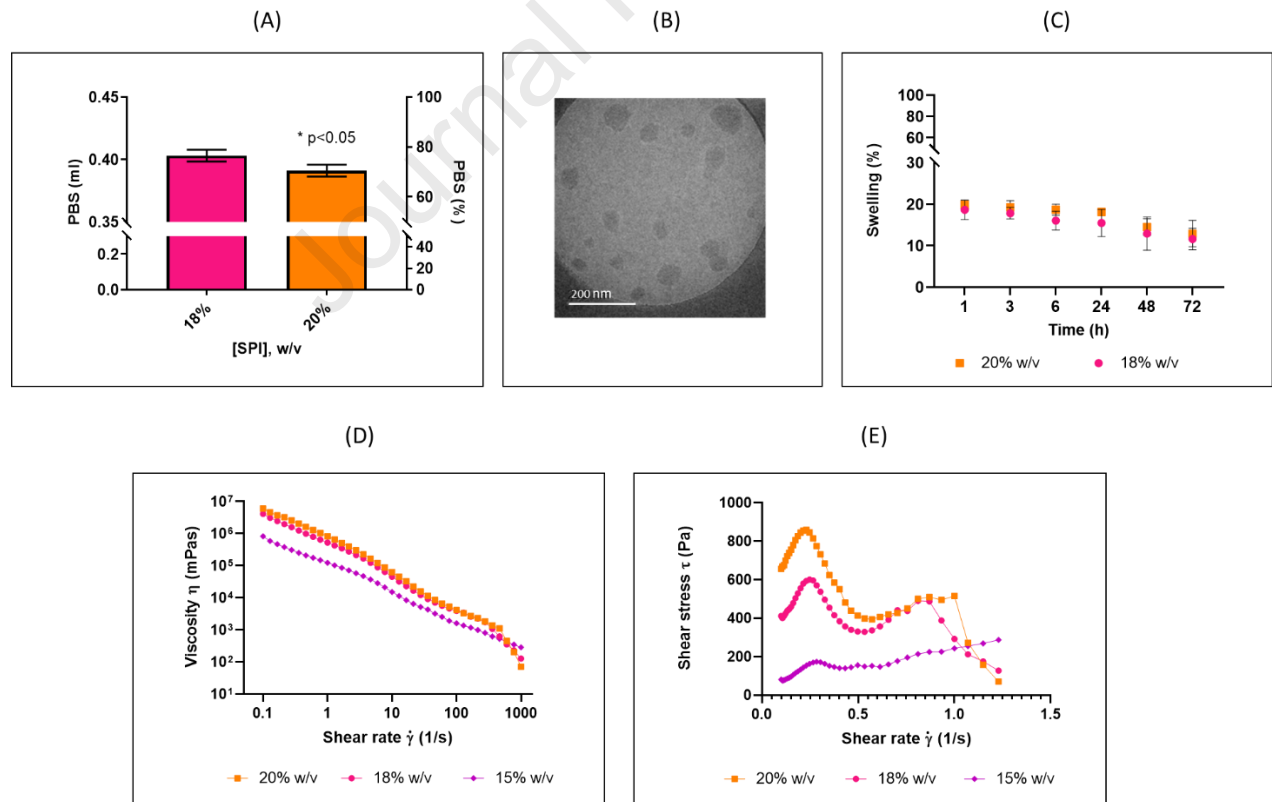
Figure 1. Characterization of hydrogels. (A) Absorption capacity of the aqueous phase by SPI powder for the formation of hydrogels at 18% w/v and 20% w/v. (B) Representative image obtained by Cryo-EM of the internal structure of the 18% w/v hydrogel. (C) Evaluation of the swelling capacity of 18% w/v and 20% w/v SPI hydrogels, at different times. (D) Alteration of the viscosity of hydrogels at 15% w/v, 18% w/v, 20% w/v SPI as the shear rate increases. (E) Flow curves diagram of hydrogels at 15% w/v, 18% w/v, 20% w/v SPI useful to determine the yield points. *Data are expressed as a mean ± standard deviation. Statistical significance was considered at p < 0.05 determined by Student's t test.*

Considering that, hopefully, these hydrogels will be implanted in a delicate biological tissue, i.e. the brain, the hydrolytic and enzymatic degradation of the biomaterial were evaluated. Both hydrogels demonstrated similar mass loss degradation profiles in D-PBS (or aCSF) over 3 days *in vitro*, reaching a maximum loss around 10% of SPI (Figure 2A). As a corroboration, we measured the total protein content of the maintaining D-PBS to confirm the lost quantity of SPI (Supplementary Fig. 2).

Considering that glycinin and β-conglycinin are the major components of the SPI [53],we checked the enzymatic degradation of hydrogels using KLK6, a secreted serine protease abundantly expressed in the central nervous system [39,40,54], and also present in mouse brain where hydrogels will be tested (Supplementary Fig. 3). Results showed that KLK6, used at a concentration comparable to that of the brain [40], was able to increase the hydrogels degradation in comparison to the hydrolytic ones (Figure 2B, C). No differences were detected between 18 and 20 % w/v hydrogels (data not shown).
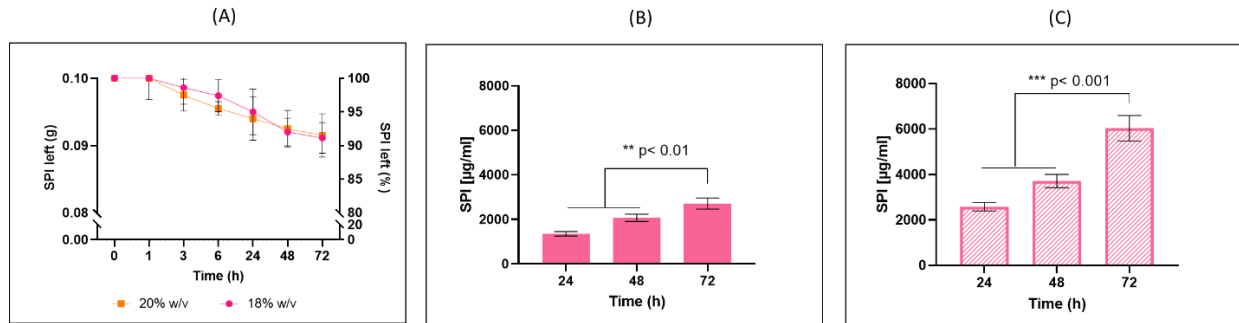
Figure 2. Degradation of hydrogels. *(A) Hydrolytic degradation of hydrogels over time, determined by measuring the loss of hydrogels weight over time, maintaining hydrogels in D-PBS or aCSF at 37°C. (B) Amount of SPI released from hydrolytic degradation of 20% SPI hydrogels over time, maintaining hydrogels in D-PBS or aCSF at 37°C. (C) Amount of SPI released from 20% SPI hydrogels in presence of KLK6 over time. Data are expressed as a mean ± standard deviation. Statistical significance was considered at p < 0.05 determined by Student's t test.*

The biodegradability feature of these hydrogels represents an advantage in the interstitial therapy, because it will not require a second surgery to remove the biomaterial, but it will be physiologically eliminated. Moreover, considering the degradation rate of hydrogels, it is possible to speculate that they will be completely eliminated within 2 months after implantation. However, improvements in the fabrication protocol will be further investigated in order to control hydrogels' degradation over time.

The SPI released from hydrogel after 24 h of hydrolytic degradation has been used to treat U87-MG and NHA cells to evaluate the potential cytotoxicity. The results (Supplementary Fig. 4A, B) showed that the cell viability of both cell lines was not reduced by SPI treatment, confirming the biocompatibility of the material. This is in accordance to the already investigated *in vivo* biocompatibility features of 18% w/v SPI hydrogels [32]. Moreover, measuring the GFAP levels,

no significant differences were detected between untreated or treated NHA cells (Supplementary Fig. 4C), suggesting that SPI did not induce astrogliosis *in vitro*.

In the forecast to exploit the biomaterial herein fabricated as a platform to control the nanomedicines release, liposomes were embedded into hydrogels as a model of drug delivery system. We have selected liposomes because it has been previously reported that they do not affect the physico-mechanical features of hydrogel [55]. Conventional liposomes of size ranging from 50 to 400 nm were prepared. A representative cryo-EM image of 100-nm sized liposomes is shown in Figure 3A. The image reveals spherical, unilamellar vesicles homogeneously distributed in vitreous ice, with diameters ranging from 80 to 120 nm.

The physico-chemical characterization (Figure 3B) showed that liposomes had a uniform size distribution (PDI ≤ 0.2) with a diameter that reflects the pores size of the extrusion filters. The ζ-potential measurement showed that the net surface charge of liposomes was negative ($< - 20$ mV). This suggests that the dispersions are stable and not prone to aggregation [56].Moreover, monitoring the liposomes size by DLS no significant changes in diameter was detected upon incubation in D-PBS or aCSF for up to 5 days, indicating the stability of the liposomes dispersion accordingly to data present in literature [57]. This is probably due to the present of cholesterol that exerts a vital role in the stability of the liposomal membrane [58].
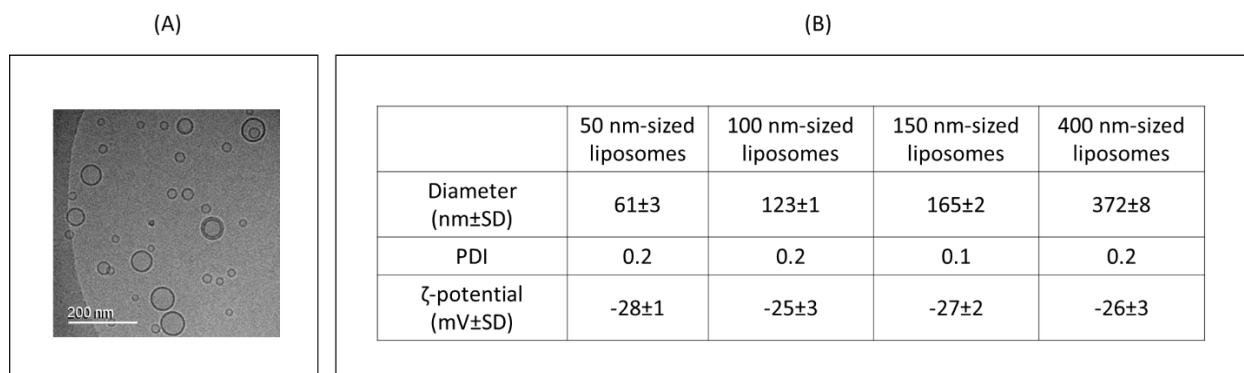
(A)

(B)

	50 nm-sized liposomes	100 nm-sized liposomes	150 nm-sized liposomes	400 nm-sized liposomes
Diameter (nm±SD)	61±3	123±1	165±2	372±8
PDI	0.2	0.2	0.1	0.2
ζ-potential (mV±SD)	-28±1	-25±3	-27±2	-26±3

Figure 3. Characterization of liposomes. (A) Representative cryoEM image of 100-nm sized liposomes. (B) Physicochemical parameters of liposomes measured by DLS and Z-Pals devices. *Data are expressed as a mean ± standard deviation.*

The Operetta CLS imaging of the hydrogel shows that fluorescent labelled liposomes displayed a homogeneous distribution within the scaffold without any significant aggregation being visualized (Figure 4). Similar liposomal distribution was previously observed in chitosan/gelatin hydrogels by Ciobanu et al. [59] and in gelatin methacryloyl hydrogels [60].
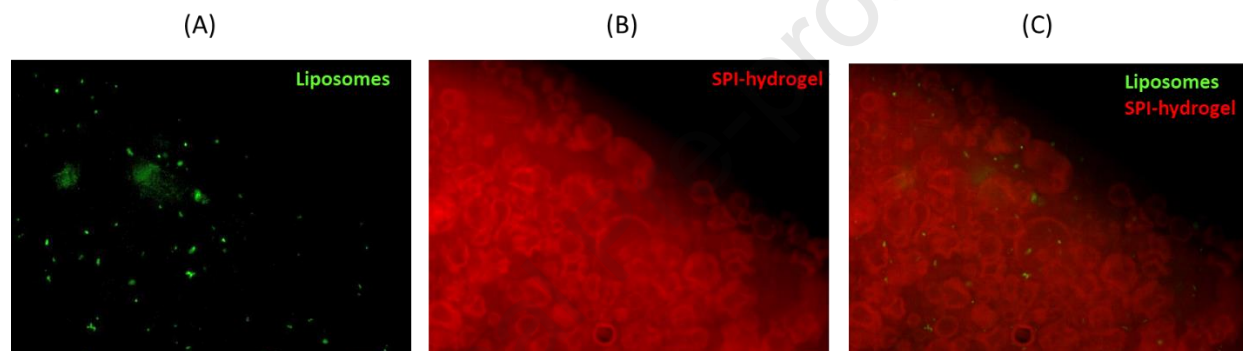

Figure 4. Operetta CLS imaging of Bodipy-labeled liposomes embedded in a 20% w/v SPI-hydrogel observed at 20 × magnification. (A) Green channel: liposomes-bodipy. (B) Red Channel: SPI hydrogels prepared using Rhodamine-D-PBS. (C) Merge of the two signals.

Hydrogels loaded with liposomes were submerged in D-PBS and incubated at 37°C. After 24 h, the D-PBS was collected and the amount of released liposomes was measured by Nanoparticle Tracking Analysis. In this way, it is possible to determine the integrity of liposomes on the base of their size.

The results showed that the release of liposomes decreased with the increase of their size for both hydrogels tested (Figure 5). Comparing the release of 50 nm liposomes between the two hydrogels

tested, a lower release (-15±5%) was measured from 20% w/v hydrogels, suggesting that the higher SPI concentration can affect the hydrogel architecture. In general, 50-nm sized liposomes were almost completely released in 24 h, whereas the release of 400-nm sized liposomes was negligible. Calculating the diffusion coefficient, which depends on the radius of liposomes and the viscosity of the hydrogel, we can infer that liposomes are continuously released by diffusion or by degradation of the biomaterial since their rate is included between 10^{-18} and 10^{-19} m^2 s^{-1}, much slower in comparison to the diffusion coefficient of drugs or liposomes from polymer-based hydrogels, that is approximately between 10^{-12} and 10^{-8} m^2 s^{-1} [61,62]. Contrarily to <150-nm liposomes that were released by diffusion, 400-nm sized liposomes were released by hydrolytic degradation.

These results suggest that combining the liposomes size with the % of SPI, it is possible to design a hybrid biomaterial system for controlled and sustained nanoparticles release, contributing to address various biological and medical challenges [63]. Furthermore, these results confirm that that the particle size has great impact on their diffusion efficiency [64].

Moreover, since liposomes are released intact, we can speculate that the hydrogel provides a protective layer for encapsulated liposomes preventing the liposomes degradations, as suggested for other liposome-in gel systems [65,66]
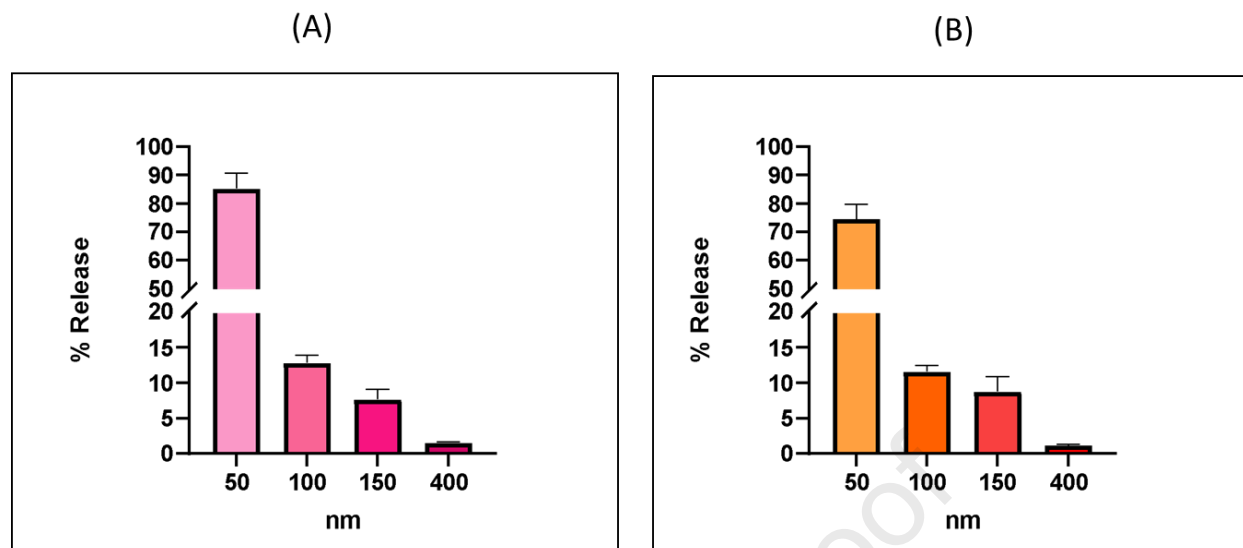
(A)   (B)

Figure 5. Release of liposomes from hydrogels. (A) Release rates of liposomes with different diameters (50, 100, 150, 400 nm) from 18% SPI hydrogels in 24 h, at 37°C. Data are expressed as a mean ± standard deviation. $F_{(4, 10)}$ = 577.2; p>0.001. (B) Release rates of liposomes with different diameter (50, 100, 150, 400 nm) from hydrogels at 20% SPI in 24 h, at 37°C. $F_{(4, 10)}$ = 490.7; p<0.0001. These results were obtained by measuring the number of liposomes released by NanoSight technology.

Finally, to verify if liposomes released from the hydrogels were pharmacologically active we fabricated hydrogels embedding liposomes loaded with the chemotherapeutic doxorubicin (LIPO-DOX), as a model. As shown in Figure 6A, entrapped DOX induce a change in liposomal shape, resulting in a characteristic "coffee bean"-structure, similarly to data present in literature [67]. LIPO-DOX showed a diameter of about 130 nm, were monodispersed and negatively charged. The encapsulation efficiency (EE %) was about 94 %, with a drug/lipid ratio of 0.3 nmol drug/µmol lipids (Figure 6B).

The amount of LIPO-DOX released from hydrogels over time was estimated by measuring the DOX fluorescence and the number of liposomes by NTA in the D-PBS were hydrogels were

22

submerged. The results (Figure 6C, D) showed that in the first 48 h liposomes were progressively released overtime, allows us to hypothesize that the liposome release kinetics are primarily dominated by diffusional liposome efflux with negligible contributions from the hydrogel degradation. At longer times, it was detected an increase of liposomes release, up to $50\pm10\%$, probably due to the contribution of hydrolytic degradation of hydrogel. No differences were detected between the two hydrogels tested. The release profile obtained by measuring the DOX fluorescence was superimposable, confirming that liposomes are released intact from hydrogel.
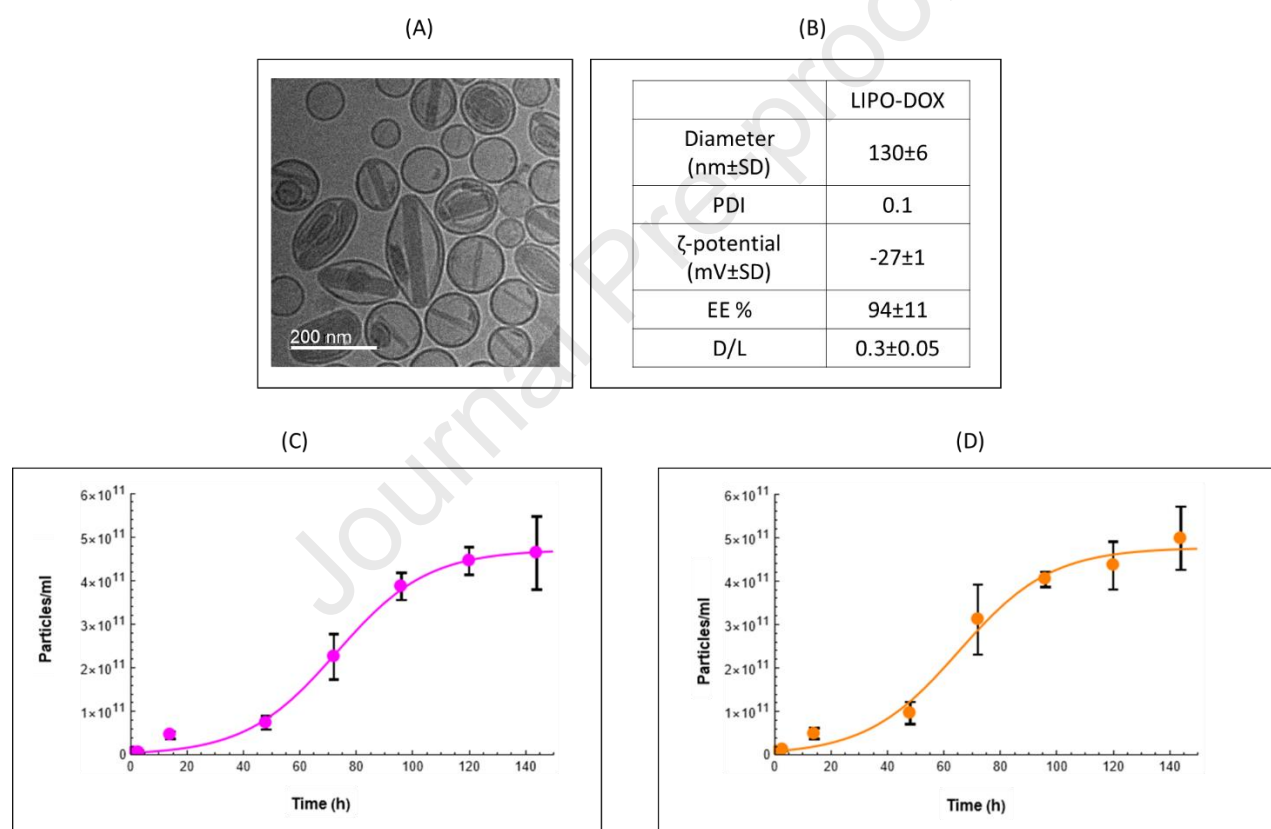

Figure 6. Characterization of doxorubicin-liposomes and their release from hydrogels. (A) Representative cryoEM image of doxorubicin-liposomes. (B) Physicochemical parameters of doxorubicin-liposomes determined by DLS and Z-Pals device. (C) Release kinetics of doxorubicin-liposomes from 18% SPI hydrogels at different times, at 37°C. (D) Release kinetics of doxorubicin-liposomes from 20% SPI hydrogels at different times, at 37°C. The continuous lines represent a fit to the data with a sigmoidal function (see text for details). These results were obtained

by measuring the number of liposomes released by NanoSight technology. Data are expressed as a mean ± standard deviation.

LIPO-DOX released from hydrogels were used to treat U87-MG cells. Cell viability was determined by MTT assay. Results showed that the cell viability decreased by increasing the LIPO-DOX concentration, suggesting that liposomes were still active in affecting cell viability after being released from hydrogel. Moreover, their effectiveness was comparable to that of original liposome samples (Figure 7). This is an important issue in the context of the design of implantable biomaterials for drug-loaded nanoparticles release, because it is important to guarantee the release of intact nanoparticles in order to control the delivery of the embed drug. This is of particularly relevance if nanoparticles are surface functionalized to target a particular cell population.
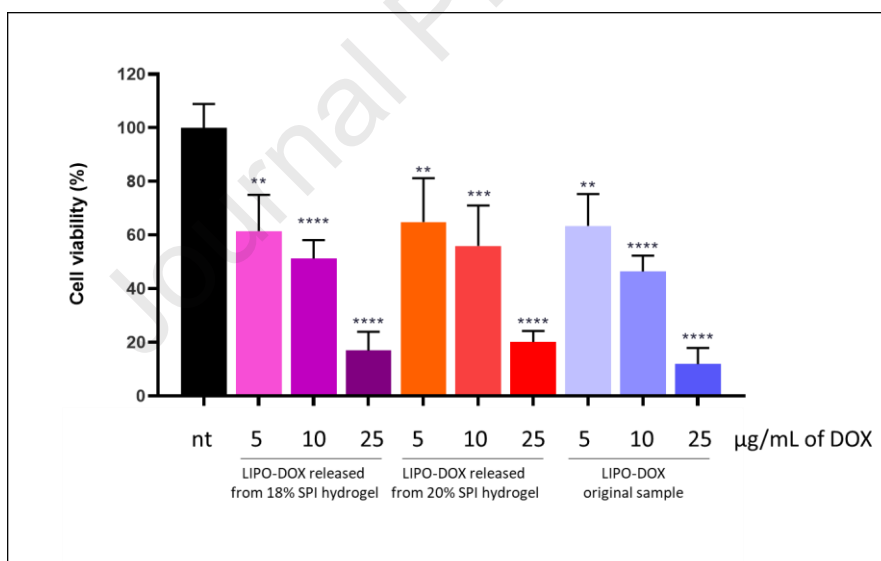

Figure 7. Cell viability of U87-MG after treatment with doxorubicin-liposomes released from hydrogels. *U87-MG cells were treated with doxorubicin-liposomes (LIPO-DOX) released from hydrogels in 24 h and cells viability was assessed by MTT assay. Cells were treated with different doses of doxorubicin (DOX) embedded in liposomes released from hydrogels. Doxorubicin-liposomes (original sample) not released from hydrogels were used as a control.* Data are expressed as a mean ± standard deviation. ***** p<0.0001, *** p<0.0002, ** p<0.002.*

24

To simulate the resected cavity as closely as possible, we developed a 3D model that mimics the shape of a hollow cylinder embedding U87-MG cells. After 5 days of culture, the hole of 3D bioprinted structures were filled with hydrogels containing plain liposomes to check the bioadhesive properties of hydrogels and the release and diffusion of liposomes (Figure 8A). Given the complexity of the 3D system, it was decided to use higher concentrations of liposomes in soy hydrogels compared to 2D studies.

The results showed that the cell viability was about 70-75%, thus confirming the biocompatibility of the implant (Figure 8B). Furthermore, it is possible to qualitative observe a greater cellular uptake of liposomes (in red) already after 24 hours of incubation, confirming the ability of hydrogels to release liposomes and that they are able to diffuse from hydrogels, targeting GB cells in a model with a complex extracellular matrix-like network and a 3D structural organization (Figure 8C). Culturing U87-MG cells in 3D can better mimic what happens *in vivo*, which makes it possible to study behavior in a more natural environment [68,69]

A weak adhesiveness of the hydrogel within this 3D model was noticed, probably due to the 3D morphology of the model and the hydration of the construct in which it was injected. This issue deserves further investigations.
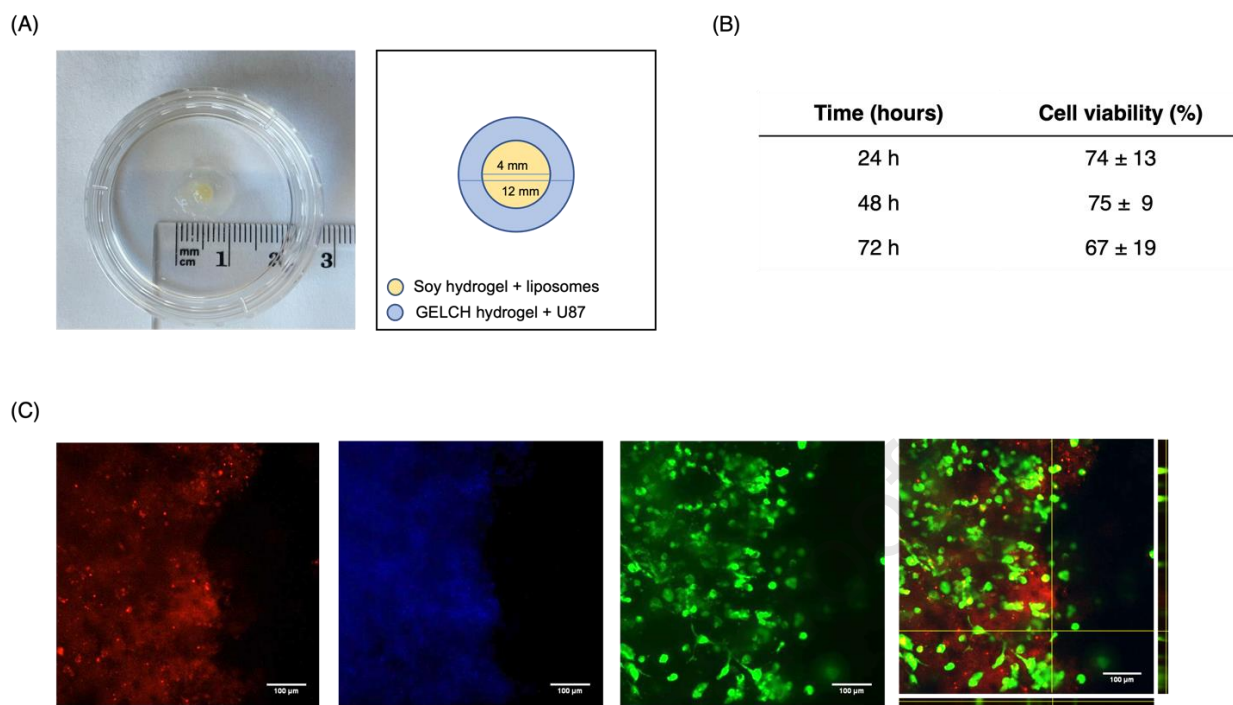
(A)

(B)

Time (hours)	Cell viability (%)
24 h	74 ± 13
48 h	75 ± 9
72 h	67 ± 19

(C)

Figure 8. Proof-of-concept in vitro using 3D-bioprinted model. *(A) Image and graphical representation of a 3D model of GELCH hydrogel composed of gelatin-chitosan and U87-MG cells, at the center of which an 18% SPI hydrogel containing LIPO-ROD was added. (B) Summary table of cell viability % at three different time-point. Data are presented as average of cell viability % ± SD, with n ≥ 8. (C) Images obtained by confocal microscopy at 24 h. Cell nuclei are marked in blue; liposomes in red; live cells in green. The last panel represents an orthogonal view of bioprinted construct obtained by Fiji ImageJ (merged signals; in yellow the co-localization between tumor cells and liposomes released from hydrogels).*

4. Conclusions

Liposomes loaded with a model drug, doxorubicin, were entrapped in SPI-based hydrogels to control the release profile of the nanomedicine with the future aim to have an implantable biomaterial useful to treat GB relapse, with biodegradability and biocompatibility features. It has been shown that SPI hydrogels possess gelling times and temperatures appropriate to the intended use, the gelation process occurs in the absence of chemicals and they are biocompatible and biodegradable. By modulating the different parameters of the system (% of SPI and liposomes

size), it is possible to obtain a sustained delivery of intact and active doxorubicin-liposomes. The versatility of liposomes (different sizes, different composition, different lamellarity, different surface functionalization) and hydrogel biomaterials (the % of SPI, the in situ gelling features) will give the possibility to fine tune the design of these systems to be used whenever controlled drug release is required. However, different aspects need to be improved. Future studies will focus on investigating the possible interaction between the cells of the central nervous system (healthy cells, cells in the tumor microenvironment, matrix components) and the hydrogel. Moreover, the validation of the implant in animal models will be necessary.

Author Contributions

F.R., F.V., L.L. and M.Ciprandi. designed research experiments, supervised the study, and wrote the manuscript. F.V., L.L. and M.Ciprandi. fabricated hydrogels, performed the characterization experiments and analyzed the data. M.K. performed cryoEM experiments and analyzed data. F.M. analyzed data to obtain the kinetic release of hydrogel. L.S. and M.C. performed rheological tests. F.V., L.L. and F.M. analyzed rheological data. S.S. and A.R. prepared and characterized liposomes. G.S. performed MTT assay on U87-MG cells. F.B. and L.R. performed the experiments with 3D *in vitro* models and analyzed data. F.R., F.V. and M.Ciprandi contributed intellectual input and data analysis. All authors discussed the data and contributed to manuscript revision. F.R. conceived the study and provided the funding. All authors agree to be accountable for all aspects of the work meet the criteria for authorship.

Declaration of competing interest

The authors declare that they have no known competing financial interests or personal relationships that could have appeared to influence the work reported in this paper.

Data statement

Data will be made available on request.

REFERENCES

[1]   S. Grochans, A.M. Cybulska, D. Simińska, J. Korbecki, K. Kojder, D. Chlubek, I. Baranowska-Bosiacka, Epidemiology of Glioblastoma Multiforme–Literature Review, Cancers (Basel) 14 (2022) 2412. https://doi.org/10.3390/cancers14102412.

[2]   R. Stupp, W.P. Mason, M.J. van den Bent, M. Weller, B. Fisher, M.J.B. Taphoorn, K. Belanger, A.A. Brandes, C. Marosi, U. Bogdahn, J. Curschmann, R.C. Janzer, S.K. Ludwin, T. Gorlia, A. Allgeier, D. Lacombe, J.G. Cairncross, E. Eisenhauer, R.O. Mirimanoff, Radiotherapy plus Concomitant and Adjuvant Temozolomide for Glioblastoma, New England Journal of Medicine 352 (2005) 987–996. https://doi.org/10.1056/NEJMoa043330.

[3]   E. Lee, R.L. Yong, P. Paddison, J. Zhu, Comparison of glioblastoma (GBM) molecular classification methods, Semin Cancer Biol 53 (2018) 201–211. https://doi.org/10.1016/j.semcancer.2018.07.006.

[4]   J.P. Fisher, D.C. Adamson, Current FDA-Approved Therapies for High-Grade Malignant Gliomas., Biomedicines 9 (2021). https://doi.org/10.3390/biomedicines9030324.

[5]   J.-M. Lemée, A. Clavreul, P. Menei, Intratumoral heterogeneity in glioblastoma: don't forget the peritumoral brain zone, Neuro Oncol 17 (2015) 1322–1332. https://doi.org/10.1093/neuonc/nov119.

[6]   C.D. Arvanitis, G.B. Ferraro, R.K. Jain, The blood–brain barrier and blood–tumour barrier in brain tumours and metastases, Nat Rev Cancer 20 (2020) 26–41. https://doi.org/10.1038/s41568-019-0205-x.

[7]   P. Ballabh, A. Braun, M. Nedergaard, The blood–brain barrier: an overview, Neurobiol Dis 16 (2004) 1–13. https://doi.org/10.1016/j.nbd.2003.12.016.

[8]   Y. Barenholz, Doxil®--the first FDA-approved nano-drug: lessons learned., J Control Release 160 (2012) 117–34. https://doi.org/10.1016/j.jconrel.2012.03.020.

[9]   P. Liu, G. Chen, J. Zhang, A Review of Liposomes as a Drug Delivery System: Current Status of Approved Products, Regulatory Environments, and Future Perspectives., Molecules 27 (2022). https://doi.org/10.3390/molecules27041372.

[10]   D.J. Lundy, H. Nguyễn, P.C.H. Hsieh, Emerging Nano-Carrier Strategies for Brain Tumor Drug Delivery and Considerations for Clinical Translation, Pharmaceutics 13 (2021) 1193. https://doi.org/10.3390/pharmaceutics13081193.

[11]   L.-L. Bu, J. Yan, Z. Wang, H. Ruan, Q. Chen, V. Gunadhi, R.B. Bell, Z. Gu, Advances in drug delivery for post-surgical cancer treatment, Biomaterials 219 (2019) 119182. https://doi.org/10.1016/j.biomaterials.2019.04.027.

[12]   S. Talebian, J. Foroughi, S.J. Wade, K.L. Vine, A. Dolatshahi-Pirouz, M. Mehrali, J. Conde, G.G. Wallace, Biopolymers for Antitumor Implantable Drug Delivery Systems: Recent Advances and Future Outlook, Advanced Materials 30 (2018). https://doi.org/10.1002/adma.201706665.

[13]   D. Di Mascolo, A.L. Palange, R. Primavera, F. Macchi, T. Catelani, F. Piccardi, R. Spanò, M. Ferreira, R. Marotta, A. Armirotti, A.L. Gallotti, R. Galli, C. Wilson, G.A. Grant, P. Decuzzi, Conformable hierarchically engineered polymeric micromeshes enabling combinatorial therapies in brain tumours, Nat Nanotechnol 16 (2021) 820–829. https://doi.org/10.1038/s41565-021-00879-3.

[14]   A. Djoudi, R. Molina-Peña, N. Ferreira, I. Ottonelli, G. Tosi, E. Garcion, F. Boury, Hyaluronic Acid Scaffolds for Loco-Regional Therapy in Nervous System Related Disorders, Int J Mol Sci 23 (2022) 12174. https://doi.org/10.3390/ijms232012174.

[15]   J. Li, D.J. Mooney, Designing hydrogels for controlled drug delivery., Nat Rev Mater 1 (2016). https://doi.org/10.1038/natrevmats.2016.71.

[16]   T.A. Juratli, G. Schackert, D. Krex, Current status of local therapy in malignant gliomas--a clinical review of three selected approaches., Pharmacol Ther 139 (2013) 341–58. https://doi.org/10.1016/j.pharmthera.2013.05.003.

[17]   J. Perry, A. Chambers, K. Spithoff, N. Laperriere, Gliadel wafers in the treatment of malignant glioma: a systematic review., Curr Oncol 14 (2007) 189–94. https://doi.org/10.3747/co.2007.147.

[18] Y. Mou, P. Zhang, W.-F. Lai, D. Zhang, Design and applications of liposome-in-gel as carriers for cancer therapy., Drug Deliv 29 (2022) 3245–3255. https://doi.org/10.1080/10717544.2022.2139021.

[19] C. Bastiancich, P. Danhier, V. Préat, F. Danhier, Anticancer drug-loaded hydrogels as drug delivery systems for the local treatment of glioblastoma, Journal of Controlled Release 243 (2016) 29–42. https://doi.org/10.1016/j.jconrel.2016.09.034.

[20] A. Turek, K. Stoklosa, A. Borecka, M. Paul-Samojedny, B. Kaczmarczyk, A. Marcinkowski, J. Kasperczyk, Designing Biodegradable Wafers Based on Poly(L-lactide-co-glycolide) and Poly(glycolide-co-ε-caprolactone) for the Prolonged and Local Release of Idarubicin for the Therapy of Glioblastoma Multiforme., Pharm Res 37 (2020) 90. https://doi.org/10.1007/s11095-020-02810-2.

[21] L. Ding, Q. Wang, M. Shen, Y. Sun, X. Zhang, C. Huang, J. Chen, R. Li, Y. Duan, Thermoresponsive nanocomposite gel for local drug delivery to suppress the growth of glioma by inducing autophagy., Autophagy 13 (2017) 1176–1190. https://doi.org/10.1080/15548627.2017.1320634.

[22] C. Bastiancich, J. Bianco, K. Vanvarenberg, B. Ucakar, N. Joudiou, B. Gallez, G. Bastiat, F. Lagarce, V. Préat, F. Danhier, Injectable nanomedicine hydrogel for local chemotherapy of glioblastoma after surgical resection., J Control Release 264 (2017) 45–54. https://doi.org/10.1016/j.jconrel.2017.08.019.

[23] T. Ozeki, D. Kaneko, K. Hashizawa, Y. Imai, T. Tagami, H. Okada, Combination therapy of surgical tumor resection with implantation of a hydrogel containing camptothecin-loaded poly(lactic-co-glycolic acid) microspheres in a C6 rat glioma model., Biol Pharm Bull 35 (2012) 545–50. https://doi.org/10.1248/bpb.35.545.

[24] L.C.S. Erthal, Y. Shi, K.J. Sweeney, O.L. Gobbo, E. Ruiz-Hernandez, Nanocomposite formulation for a sustained release of free drug and drug-loaded responsive nanoparticles: an approach for a local therapy of glioblastoma multiforme., Sci Rep 13 (2023) 5094. https://doi.org/10.1038/s41598-023-32257-5.

[25] Y. Ni, W. Zhao, W. Cheng, C. Deng, Z. Ying, L. Li, X. Wang, C. Sun, J. Tu, L. Jiang, Lipopeptide liposomes-loaded hydrogel for multistage transdermal chemotherapy of melanoma., J Control Release 351 (2022) 245–254. https://doi.org/10.1016/j.jconrel.2022.09.014.

[26] R. Mokdad, A. Aouabed, V. Ball, F.F. Si Youcef, N. Nasrallah, B. Heurtault, A. HadjSadok, Formulation and rheological evaluation of liposomes-loaded carbopol hydrogels based on thermal waters., Drug Dev Ind Pharm 48 (2022) 635–645. https://doi.org/10.1080/03639045.2022.2152044.

[27] B.R. Thompson, B.C. Zarket, E.H. Lauten, S. Amin, S. Muthukrishnan, S.R. Raghavan, Liposomes Entrapped in Biopolymer Hydrogels Can Spontaneously Release into the External Solution., Langmuir 36 (2020) 7268–7276. https://doi.org/10.1021/acs.langmuir.0c00596.

[28] D. Cao, X. Zhang, M.D. Akabar, Y. Luo, H. Wu, X. Ke, T. Ci, Liposomal doxorubicin loaded PLGA-PEG-PLGA based thermogel for sustained local drug delivery for the treatment of breast cancer., Artif Cells Nanomed Biotechnol 47 (2019) 181–191. https://doi.org/10.1080/21691401.2018.1548470.

[29] H. Karimi, S. Rabbani, D. Babadi, S. Dadashzadeh, A. Haeri, Piperine liposome-embedded in hyaluronan hydrogel as an effective platform for prevention of postoperative peritoneal adhesion., J Microencapsul 40 (2023) 279–301. https://doi.org/10.1080/02652048.2023.2194415.

[30] Y. Liu, Y. Cui, M. Liao, pH- and temperature-responsive IPN hydrogels based on soy protein and poly(N -isopropylacrylamide- co -sodium acrylate), J Appl Polym Sci 131 (2014) n/a-n/a. https://doi.org/10.1002/app.39781.

[31] A. Abaee, M. Mohammadian, S.M. Jafari, Whey and soy protein-based hydrogels and nano-hydrogels as bioactive delivery systems, Trends Food Sci Technol 70 (2017) 69–81. https://doi.org/10.1016/j.tifs.2017.10.011.

[32] K.B. Chien, E.J. Chung, R.N. Shah, Investigation of soy protein hydrogels for biomedical applications: Materials characterization, drug release, and biocompatibility, J Biomater Appl 28 (2014) 1085–1096. https://doi.org/10.1177/0885328213497413.

[33] Artificial Cerebrospinal Fluid (ACSF) (1×)., Cold Spring Harb Protoc 2017 (2017). https://doi.org/10.1101/pdb.rec094359.

[34] A. Albini, [Standardization of a method of determining the thiolic-SH groups in human blood due to kinetic considerations]., Boll Soc Ital Biol Sper 56 (1980) 1892–8.

[35] T. Mezger, Applied Rheology – With Joe Flow on Rheology Road, 2020th ed., GmbH, 2020.

[36] G. V. Vinogradov, A. Ya. Malkin, Rheological properties of polymer melts, Journal of Polymer Science Part A-2: Polymer Physics 4 (1966) 135–154. https://doi.org/10.1002/pol.1966.160040111.

[37] A. Pope, R.A. Nixon, Proteases of human brain, Neurochem Res 9 (1984) 291–323. https://doi.org/10.1007/BF00963980.

[38] J.L. Molinuevo, S. Ayton, R. Batrla, M.M. Bednar, T. Bittner, J. Cummings, A.M. Fagan, H. Hampel, M.M. Mielke, A. Mikulskis, S. O'Bryant, P. Scheltens, J. Sevigny, L.M. Shaw, H.D. Soares, G. Tong, J.Q. Trojanowski, H. Zetterberg, K. Blennow, Current state of Alzheimer's fluid biomarkers, Acta Neuropathol 136 (2018) 821–853. https://doi.org/10.1007/s00401-018-1932-x.

[39] K. Murakami, Y.-P. Jiang, T. Tanaka, Y. Bando, B. Mitrovic, S. Yoshida, In vivo analysis of kallikrein-related peptidase 6 (KLK6) function in oligodendrocyte development and the expression of myelin proteins, Neuroscience 236 (2013) 1–11. https://doi.org/10.1016/j.neuroscience.2012.12.073.

[40] E.P. Diamandis, G.M. Yousef, C. Petraki, A.R. Soosaipillai, Human Kallikrein 6 as a Biomarker of Alzheimer's Disease, Clin Biochem 33 (2000) 663–667. https://doi.org/10.1016/S0009-9120(00)00185-5.

[41] F. Re, I. Cambianica, S. Sesana, E. Salvati, A. Cagnotto, M. Salmona, P.-O. Couraud, S.M. Moghimi, M. Masserini, G. Sancini, Functionalization with ApoE-derived peptides enhances the interaction with brain capillary endothelial cells of nanoliposomes binding amyloid-beta peptide, J Biotechnol 156 (2011) 341–346. https://doi.org/10.1016/j.jbiotec.2011.06.037.

[42] M. Pizzocri, F. Re, E. Stanzani, B. Formicola, M. Tamborini, E. Lauranzano, F. Ungaro, S. Rodighiero, M. Francolini, M. Gregori, A. Perin, F. DiMeco, M. Masserini, M. Matteoli, L. Passoni, Radiation and adjuvant drug-loaded liposomes target glioblastoma stem cells and trigger in-situ immune response, Neurooncol Adv 3 (2021). https://doi.org/10.1093/noajnl/vdab076.

[43] S. Giofrè, A. Renda, S. Sesana, B. Formicola, B. Vergani, B.E. Leone, V. Denti, G. Paglia, S. Groppuso, V. Romeo, L. Muzio, A. Balboni, A. Menegon, A. Antoniou, A. Amenta, D. Passarella, P. Seneci, S. Pellegrino, F. Re, Dual Functionalized Liposomes for Selective Delivery of Poorly Soluble Drugs to Inflamed Brain Regions, Pharmaceutics 14 (2022) 2402. https://doi.org/10.3390/pharmaceutics14112402.

[44] G. Sierri, R. Dal Magro, B. Vergani, B.E. Leone, B. Formicola, L. Taiarol, S. Fagioli, M. Kravicz, L. Tremolizzo, L. Calabresi, F. Re, Reduced Levels of ABCA1 Transporter Are Responsible for the Cholesterol Efflux Impairment in β-Amyloid-Induced Reactive Astrocytes: Potential Rescue from Biomimetic HDLs., Int J Mol Sci 23 (2021). https://doi.org/10.3390/ijms23010102.

[45] S. Magli, G.B. Rossi, G. Risi, S. Bertini, C. Cosentino, L. Crippa, E. Ballarini, G. Cavaletti, L. Piazza, E. Masseroni, F. Nicotra, L. Russo, Design and Synthesis of Chitosan—Gelatin Hybrid Hydrogels for 3D Printable in vitro Models, Front Chem 8 (2020). https://doi.org/10.3389/fchem.2020.00524.

[46] M. Vomero, F. Ciarpella, E. Zucchini, M. Kirsch, L. Fadiga, T. Stieglitz, M. Asplund, On the longevity of flexible neural interfaces: Establishing biostability of polyimide-based intracortical implants, Biomaterials 281 (2022) 121372. https://doi.org/10.1016/j.biomaterials.2022.121372.

[47] R.F. Keep, Y. Hua, G. Xi, Brain Water Content: a Misunderstood Measurement?, Transl Stroke Res 3 (2012) 263–265. https://doi.org/10.1007/s12975-012-0152-2.

[48] C. Hu, L. Hahn, M. Yang, A. Altmann, P. Stahlhut, J. Groll, R. Luxenhofer, Improving printability of a thermoresponsive hydrogel biomaterial ink by nanoclay addition, J Mater Sci 56 (2021) 691–705. https://doi.org/10.1007/s10853-020-05190-5.

[49] N. Paxton, W. Smolan, T. Böck, F. Melchels, J. Groll, T. Jungst, Proposal to assess printability of bioinks for extrusion-based bioprinting and evaluation of rheological properties governing bioprintability., Biofabrication 9 (2017) 044107. https://doi.org/10.1088/1758-5090/aa8dd8.

[50] R.R. Vildanova, N.N. Sigaeva, O.S. Kukovinets, S.V. Kolesov, Preparation and rheological properties of hydrogels based on N-succinyl chitosan and hyaluronic acid dialdehyde, Polym Test 96 (2021) 107120. https://doi.org/10.1016/j.polymertesting.2021.107120.

[51] W.J. Polacheck, I.K. Zervantonakis, R.D. Kamm, Tumor cell migration in complex microenvironments, Cellular and Molecular Life Sciences 70 (2013) 1335–1356. https://doi.org/10.1007/s00018-012-1115-1.

[52] A.J. Engler, S. Sen, H.L. Sweeney, D.E. Discher, Matrix Elasticity Directs Stem Cell Lineage Specification, Cell 126 (2006) 677–689. https://doi.org/10.1016/j.cell.2006.06.044.

[53] M. Keerati-u-rai, M. Miriani, S. Iametti, F. Bonomi, M. Corredig, Structural changes of soy proteins at the oil–water interface studied by fluorescence spectroscopy, Colloids Surf B Biointerfaces 93 (2012) 41–48. https://doi.org/10.1016/j.colsurfb.2011.12.002.

[54] F.X. Gomis-Rüth, Á. Bayés, G. Sotiropoulou, G. Pampalakis, T. Tsetsenis, V. Villegas, F.X. Avilés, M. Coll, The Structure of Human Prokallikrein 6 Reveals a Novel Activation Mechanism for the Kallikrein Family, Journal of Biological Chemistry 277 (2002) 27273–27281. https://doi.org/10.1074/jbc.M201534200.

[55] S. Correa, A.K. Grosskopf, J.H. Klich, H.L. Hernandez, E.A. Appel, Injectable Liposome-based Supramolecular Hydrogels for the Programmable Release of Multiple Protein Drugs., Matter 5 (2022) 1816–1838. https://doi.org/10.1016/j.matt.2022.03.001.

[56] G. Bozzuto, A. Molinari, Liposomes as nanomedical devices., Int J Nanomedicine 10 (2015) 975–99. https://doi.org/10.2147/IJN.S68861.

[57] L. Bana, S. Minniti, E. Salvati, S. Sesana, V. Zambelli, A. Cagnotto, A. Orlando, E. Cazzaniga, R. Zwart, W. Scheper, M. Masserini, F. Re, Liposomes bi-functionalized with phosphatidic acid and an ApoE-derived peptide affect Aβ aggregation features and cross the blood-brain-barrier: implications for therapy of Alzheimer disease., Nanomedicine 10 (2014) 1583–90. https://doi.org/10.1016/j.nano.2013.12.001.

[58] P. Nakhaei, R. Margiana, D.O. Bokov, W.K. Abdelbasset, M.A. Jadidi Kouhbanani, R.S. Varma, F. Marofi, M. Jarahian, N. Beheshtkhoo, Liposomes: Structure, Biomedical Applications, and Stability Parameters With Emphasis on Cholesterol., Front Bioeng Biotechnol 9 (2021) 705886. https://doi.org/10.3389/fbioe.2021.705886.

[59] B.C. Ciobanu, A.N. Cadinoiu, M. Popa, J. Desbrières, C.A. Peptu, Modulated release from liposomes entrapped in chitosan/gelatin hydrogels., Mater Sci Eng C Mater Biol Appl 43 (2014) 383–91. https://doi.org/10.1016/j.msec.2014.07.036.

[60] K. Elkhoury, L. Sanchez-Gonzalez, P. Lavrador, R. Almeida, V. Gaspar, C. Kahn, F. Cleymand, E. Arab-Tehrany, J.F. Mano, Gelatin Methacryloyl (GelMA) Nanocomposite Hydrogels Embedding Bioactive Naringin Liposomes., Polymers (Basel) 12 (2020). https://doi.org/10.3390/polym12122944.

[61] R. Pjanoviè, N. Bo″koviè -Vragoloviè ,J. Veljkoviè -Giga, R. Gariè -Gruloviè ,S. Pejanoviè , B. Bugarski, Diffusion of drugs from hydrogels and liposomes as drug carriers, Journal of Chemical Technology & Biotechnology 85 (2010) 693–698. https://doi.org/10.1002/jctb.2357.

[62] S. Jung, R. Song, J. Kim, J.H. Ko, J. Lee, Controlling the Release of Amphiphilic Liposomes from Alginate Hydrogel Particles for Antifouling Paint., Langmuir 36 (2020) 1515–1522. https://doi.org/10.1021/acs.langmuir.9b03415.

[63] W. Gao, Y. Zhang, Q. Zhang, L. Zhang, Nanoparticle-Hydrogel: A Hybrid Biomaterial System for Localized Drug Delivery., Ann Biomed Eng 44 (2016) 2049–61. https://doi.org/10.1007/s10439-016-1583-9.

[64] T. Furst, G.R. Dakwar, E. Zagato, A. Lechanteur, K. Remaut, B. Evrard, K. Braeckmans, G. Piel, Freeze-dried mucoadhesive polymeric system containing pegylated lipoplexes: Towards a vaginal sustained released system for siRNA., J Control Release 236 (2016) 68–78. https://doi.org/10.1016/j.jconrel.2016.06.028.

[65] J.-S. Lee, D. Chung, H.G. Lee, Preparation and characterization of calcium pectinate gel beads entrapping catechin-loaded liposomes., Int J Biol Macromol 42 (2008) 178–84. https://doi.org/10.1016/j.ijbiomac.2007.10.008.

[66] M.A. Moustafa, W.M. El-Refaie, Y.S.R. Elnaggar, O.Y. Abdallah, Gel in core carbosomes as novel ophthalmic vehicles with enhanced corneal permeation and residence., Int J Pharm 546 (2018) 166–175. https://doi.org/10.1016/j.ijpharm.2018.05.040.

[67] A. Fritze, F. Hens, A. Kimpfler, R. Schubert, R. Peschka-Süss, Remote loading of doxorubicin into liposomes driven by a transmembrane phosphate gradient., Biochim Biophys Acta 1758 (2006) 1633–40. https://doi.org/10.1016/j.bbamem.2006.05.028.

[68] R. Krencik, K. Seo, J. V. van Asperen, N. Basu, C. Cvetkovic, S. Barlas, R. Chen, C. Ludwig, C. Wang, M.E. Ward, L. Gan, P.J. Horner, D.H. Rowitch, E.M. Ullian, Systematic Three-Dimensional Coculture Rapidly Recapitulates Interactions between Human Neurons and Astrocytes, Stem Cell Reports 9 (2017) 1745–1753. https://doi.org/10.1016/j.stemcr.2017.10.026.

[69] M. Kapałczyńska, T. Kolenda, W. Przybyła, M. Zajączkowska, A. Teresiak, V. Filas, M. Ibbs, R. Bliźniak, Ł. Łuczewski, K. Lamperska, 2D and 3D cell cultures – a comparison of different types of cancer cell cultures, Archives of Medical Science (2016). https://doi.org/10.5114/aoms.2016.63743.

HIGHLIGHTS

- Glioblastoma is an aggressive brain tumour with high rate of recurrence.

- Implantable biomaterials are promising approaches against glioblastoma relapse.

- Soy protein hydrogels embedding drug-loaded liposomes were pioneering fabricated.

- Varying soy protein amount and liposome size, a controlled release is achieved.

- The liposomes released from hydrogels are intact and active on glioblastoma cells.

Declaration of interests

☒ The authors declare that they have no known competing financial interests or personal relationships that could have appeared to influence the work reported in this paper.

☐ The authors declare the following financial interests/personal relationships which may be considered as potential competing interests: